

PAPER • OPEN ACCESS

Lattice matched Volmer–Weber growth of Fe_3Si on GaAs(001)—the influence of the growth rate

To cite this article: B Jenichen *et al* 2019 *Semicond. Sci. Technol.* **34** 124002

View the [article online](#) for updates and enhancements.

You may also like

- [Modeling of the self-limited growth in catalytic chemical vapor deposition of graphene](#)
HoKwon Kim, Eduardo Saiz, Manish Chhowalla *et al.*
- [A Simple Approach to Growth Mode of InN and InGaN Thin Films on GaN\(0001\) Substrate](#)
Katsuya Nagai, Toru Akiyama, Kohji Nakamura *et al.*
- [Stability and Stirring in Crystal Growth from High Temperature Solutions](#)
Hans J. Scheel and D. Elwell



IOP | ebooks™

Bringing together innovative digital publishing with leading authors from the global scientific community.

Start exploring the collection—download the first chapter of every title for free.

Lattice matched Volmer–Weber growth of Fe₃Si on GaAs(001)—the influence of the growth rate

B Jenichen , Z Cheng , M Hanke, J Herfort and A Trampert

Paul-Drude-Institut für Festkörperelektronik Leibniz-Institut im Forschungsverbund Berlin e.V.,
Hausvogteiplatz 5-7, D-10117 Berlin, Germany

E-mail: bernd.jenichen@pdi-berlin.de

Received 16 July 2019, revised 27 August 2019

Accepted for publication 9 October 2019

Published 29 October 2019



Abstract

We investigate the formation of lattice matched single-crystalline Fe₃Si/GaAs(001) ferromagnet/semiconductor hybrid structures by Volmer–Weber island growth, starting from the epitaxial growth of isolated Fe₃Si islands up to the formation of continuous films as a result of island coalescence. We find coherent defect-free layers exhibiting compositional disorder near the Fe₃Si/GaAs—interface for higher growth rates, whereas they are fully ordered for lower growth rates.

Keywords: Volmer–Weber growth, molecular beam epitaxy, metal on semiconductor, ferromagnetic film

(Some figures may appear in colour only in the online journal)

Introduction

Often thin film growth can be realized in a layer-by-layer mode resulting in narrow interface widths. However, during heteroepitaxy of a metal film on top of a semiconductor different surface tensions of the epitaxial materials play a crucial role [1, 2]. A poor wetting of the substrate surface by the deposited metal may result in an island growth mode even for zero mismatch [3], which can be utilized for the growth of nanostructures [2, 4]. Surface energies of GaAs(001) lie in the range near 65 meV Å⁻² [5] whereas the energies of Fe₃Si(001) are in the range from 100 to 200 meV Å⁻² or even above [6], i.e. Fe₃Si has really higher surface energies compared to GaAs.

In the case of Fe₃Si growth on GaAs the stoichiometry of the metallic films has an influence on their lattice parameter [7, 8] and their long-range ordering [9]. We find three types of diffraction maxima of Fe₃Si. Fundamental reflections, i.e. $H + K + L = 4n$ (where n is integer), are not sensitive to

disorder. Their structure factor is $F_{4n} = 4(f_{\text{Si}} + 3f_{\text{Fe}})$. In the D0₃ structure of Fe₃Si the Si atoms occupy the lattice position D, whereas the Fe atoms sit on the positions A, B, C, see figure 1 [9, 10]. The disorder is described by two types of order parameters α and β , which are the fractions of Si atoms occupying the Fe(B) and the Fe(A, C) sites, respectively. For $H + K + L = 2n$ (where n is odd) the structure factor is

$$F_{2n} = -4(1 - 2\beta)(f_{\text{Si}} - f_{\text{Fe}}). \quad (1)$$

And for odd H, K, L we have

$$F_{2n+1} = 4i(1 - 2\alpha - \beta)(f_{\text{Si}} - f_{\text{Fe}}). \quad (2)$$

The lattice misfit between Fe₃Si and GaAs is minimized for stoichiometric films. The lattice parameter of GaAs is 0.56325 nm whereas the lattice parameter of Fe₃Si is 0.5654 nm [11]. From these values we obtain a mismatch below 0.4%. In earlier work we found evidence for the presence of islands: The measured island height was larger than the nominal thickness of the deposited film [3]. Later Fe₃Si islands on GaAs were directly imaged by scanning tunneling microscopy, and it was found that the islands show a D0₃ structure, i.e. they were fully ordered [12]. After coalescence



Original content from this work may be used under the terms of the Creative Commons Attribution 3.0 licence. Any further distribution of this work must maintain attribution to the author(s) and the title of the work, journal citation and DOI.

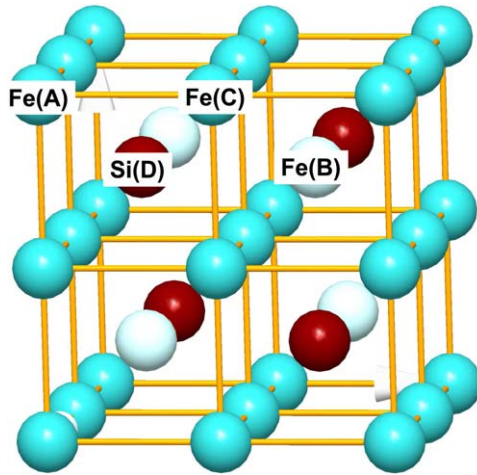


Figure 1. D₀₃ order of the Fe₃Si lattice. The Si-atoms are located on the D-position of the lattice, whereas the Fe-atoms sit on the A-, B-, and C-positions.

of the Fe₃Si islands a layer-by-layer growth of the metal was observed, which is typical for homoepitaxy of Fe₃Si [13, 14].

In general, the material Fe₃Si with its high Curie temperature of about 567 °C is well suited for spintronic applications. The spin polarization of Fe₃Si is about 45% [15]. Room temperature spin injection from Fe₃Si into GaAs was demonstrated [16]. The role of interdiffusion in the system Fe₃Si/GaAs was investigated, and influence of interdiffusion on the ordering was found [17, 18]. The ferromagnetism of the thin Fe₃Si films arises at a nominal thickness of about 3 monolayers (MLs) [12, 19, 20]. One ML corresponds to 0.28 nm.

The aim of the present work is a detailed structural characterization of the heteroepitaxial Fe₃Si on GaAs(001). We directly image Fe₃Si growth islands by cross-section high resolution transmission electron microscopy (HR TEM) and perform corresponding measurements of crystal truncation rods using grazing incidence x-ray diffraction (XRD) of synchrotron radiation. The influence of the growth rate on long-range ordering is studied. A comparison of fundamental and superlattice maxima gives information about long-range ordering within the Fe₃Si [9, 10]. Residual disordering near the Fe₃Si/GaAs interface is revealed using the Z-contrast method in a probe-C_s-corrected scanning TEM (STEM) with atomic resolution.

Experimental

The GaAs(001) substrates were overgrown with a 350 nm thick GaAs buffer layer at a growth temperature $T_G = 580$ °C. After cooling down this leads to a formation of an atomically flat and As-rich $c(4 \times 4)$ reconstructed GaAs (001) surface. Subsequently, the substrates were transferred under UHV conditions to a separate, As-free chamber with a base pressure of 1×10^{-10} mbar where the Fe₃Si was grown at different growth rates (3 ML/h and 71 ML/h). Fe and Si where coevaporated and deposited on the GaAs substrate at $T_G = 200$ °C [7, 8].

Two types of samples were compared (see table 1), i.e. samples grown with a relatively high Fe₃Si growth rate (samples 1 and 3) and samples grown with lower Fe₃Si growth rate (samples 2 and 4). Growth rates and Fe₃Si stoichiometry were determined via calibration measurements using XRD peak position and thickness fringes [8, 13]. In addition we measured reflection high energy electron diffraction oscillations and x-ray oscillations of the layer-by-layer growth of Fe₃Si. We have used these methods because the flux rates are relatively low and cannot be determined directly with the sufficient accuracy. Two different types of MBE systems were used, one with relatively low growth rate [21] due to geometrical reasons, the other with higher growth rate [7]. Two nominal Fe₃Si film thicknesses were taken into account: 3 ML (before coalescence of growth islands, samples 1 and 2) and 6 ML (after coalescence of growth islands, samples 3 and 4). Some of the samples (samples 1 and 3) were capped with 4 nm of amorphous Ge deposited at $T_G = 150$ °C, the remaining ones (samples 2 and 4) were characterized *in situ* immediately after the growth. Sample 5 contains a 36 nm thick Fe₃Si film on top of the GaAs(001) buffer layer. It was grown at high growth rate. The ordering of the thick Fe₃Si film near the Fe₃Si/GaAs interface is investigated using sample 5.

Synchrotron-based XRD was performed in grazing incidence geometry at the PHARAO U-125/2 KMC beamline of the storage ring BESSY II (Berlin). The photon energy was 10 keV, with an energy resolution of $\Delta E/E \sim 10^{-4}$. The simulations of the crystal truncation rods were performed as in [3], where the disorder parameters α and β where taken into account.

The GaAs 222 and 002 reflections are quasiforbidden and in that way the corresponding Fe₃Si maxima are not disturbed by an intense substrate reflection. In this manner the disorder parameter β can be determined with high sensitivity. In the present work we restrict ourselves to this parameter, because the amount of material is extremely small and α cannot be determined due to intense substrate contribution for odd H, K, L.

Cross-sectional TEM specimens were prepared by mechanical lapping and polishing, followed by Ar ion milling. A TEM JEOL JEM2100 F operated at 200 kV was used for high-resolution (HR) imaging. The probe-C_s-corrected JEOL ARM200 operated in the STEM mode at 200 kV was utilized for atomically resolved high-angle annular dark field (HAADF) imaging. In addition, corresponding image contrast simulations using the program JEMS allowed for a certain interpretation of the image contrast [22].

Results

Fe₃Si islands of sample 1 imaged by HR TEM (figure 2) are approximately 4 MLs high and 3 nm in lateral size. The real height of 4 MLs is larger than the nominal film thickness 3 MLs, and so the coverage of the GaAs surface becomes smaller than 1.

Figure 3 shows the L-scans of all the samples of the 20L and 22L crystal truncation rods measured by grazing incidence diffraction using synchrotron radiation. From comparison with simulations we obtain for sample 1 an island height of 4 MLs and a poor ordering of the Fe₃Si islands (with

Table 1. Nominal (measured) film thicknesses (island heights), substrate temperatures T_S , growth rates v_g during epitaxial growth, and the order parameters β determined by simulation of the x-ray diffraction L-scans for four samples investigated.

	Sample thickness (ML)	1 T_S °C	v_g (ML/h)	β	Sample thickness (ML)	2 T_S °C	v_g (ML/h)	β	Sample thickness (ML)	3 T_S °C	v_g (ML/h)	β	Sample thickness (ML)	4 T_S °C	v_g (ML/h)	β
GaAs	1071	580		./.	1071	580		./.	1071	580		./.	1071	580		./.
Fe ₃ Si	3 (4)	200	71	0.48	3 (4)	200	3	0.0	6 (7)	200	71	0.45	7 (7 ± 1)	200	3	0.0
Ge	14	150		./.	./.			./.	14	150		./.	./.			./.

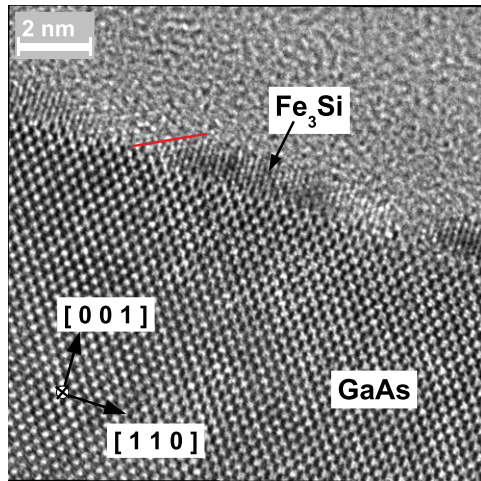


Figure 2. Cross-section high-resolution transmission electron micrograph of sample 1 with Fe_3Si islands epitaxially grown on the GaAs(001) substrate. The contact angle at the edge of the Fe_3Si island is marked by a red line.

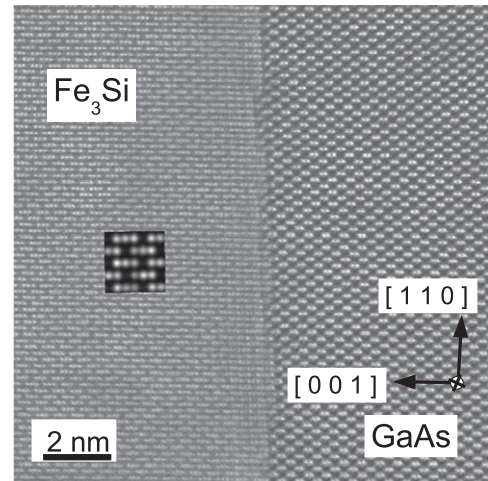


Figure 4. Cross-section high-resolution scanning transmission electron micrograph of an Fe_3Si film epitaxially grown on the GaAs (001) substrate at a growth rate of 71 ML/h detected in the high-angle annular dark field mode. Near the $\text{Fe}_3\text{Si}/\text{GaAs}$ interface we find evidence of disordering of the Fe_3Si . The inset shows a simulation for perfectly $\text{D}0_3$ ordered Fe_3Si .

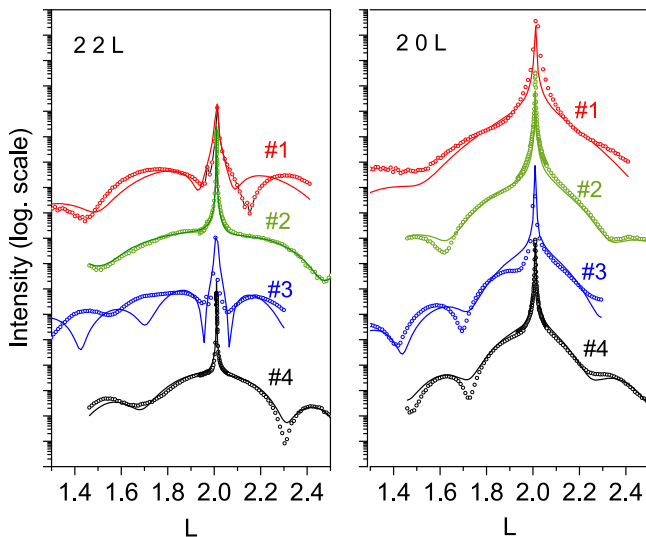


Figure 3. X-ray diffraction L-scans along the 22L (left) and 20L (right) crystal truncation rods for all samples. The symbols show the results of the experiments, the lines are the corresponding simulations. For sample 1 the intensity of the Fe_3Si 222 maximum is reduced near the GaAs 222 peak. For sample 2 we observe the full intensity of the Fe_3Si 222 maximum. For sample 3 the intensity of the Fe_3Si 222 maximum is reduced near the GaAs 222 peak, and the disorder is changing with depth. For sample 4 we observe again the full intensity of the Fe_3Si 222 maximum. The resulting order parameters and film thicknesses are given in table 1.

$\beta = 0.48$, see table 1, see also [9]). The 202 maximum is fundamental and not sensitive to disorder [9]. Therefore we determined the island height from comparison of the experimental curve and the simulation of this 20L crystal truncation rod and used the same height for the simulation of the 22L-measurement as well. Obviously for the 22L-measurement the fringe period is deviating from the calculated value indicating inhomogeneity of the ordering.

The 202 diffraction maxima of Fe_3Si and GaAs overlap without peak shift, i.e. the Fe_3Si islands exhibit nearly ideal

stoichiometry [7, 8]. For sample 1 the 222 and 002 maxima have characteristic shapes with a strong reduction of the Fe_3Si layer maxima, which are evidence for chemical disorder in the Fe_3Si . The difference with respect to a fully ordered film becomes obvious from comparison with sample 2 (figure 3). The 202 peaks of both samples are rather similar, because they are not sensitive to disorder, whereas the 222 peaks of the Fe_3Si islands differ, because in sample 1 the Fe_3Si is disordered, resulting in a reduced Fe_3Si 222 peak intensity, and in sample 2 it is fully ordered with $\beta = 0.0$ (see table 1), and the Fe_3Si 222 peak exhibits full intensity. Sample 3 contains a nominally 6 ML thick film, and was grown at high growth rate. It exhibits strong disorder with $\beta = 0.45$. For sample 3 the thickness of the disordered region again does not coincide with the full film thickness due to inhomogeneous ordering resulting in different interference period lengths for fundamental and superlattice maxima, i.e. a disagreement of measurement and simulation. Sample 4 is a nominally (7 ± 1) ML thick film, and was grown at low growth rate, and exhibits perfect ordering with $\beta = 0.0$ (see table 1). The measured thickness for this sample coincides with the nominal thickness, i.e. the coverage now equals one. The film is continuous now, all islands are coalesced. This would be the starting phase of Fe_3Si homoepitaxy.

Figure 4 shows the $\text{Fe}_3\text{Si}/\text{GaAs}$ interface of sample 5 in a scanning transmission micrograph taken in the HAADF mode of the STEM. The inset depicts a simulation for perfectly $\text{D}0_3$ ordered Fe_3Si with characteristic Fe-triples. In the z -contrast mode the Fe atoms give the highest scattering intensity, whereas the Si atoms scatter with lower intensity [23]. The GaAs crystal structure is nearly ideal, however the Fe_3Si structure shows evidence of disordering near the interface, where the Fe-triples are blurred. The sample was grown at a growth rate of 71 ML/h. The disordering near the interface is connected to the disorder occurring during the starting phase of the epitaxial growth. We

note, that a similar effect was obtained for the growth of lattice matched Co_2FeSi Heusler alloy film on GaAs(001) [24]. The role of interdiffusion should be stronger for lower growth rate, however, perfect ordering is found for the lower growth rate. In this way the disorder found in our case is rather a growth phenomenon.

Neglecting the anisotropy of Fe_3Si we can make a rough estimate of the $\text{Fe}_3\text{Si}/\text{GaAs}(001)$ interface energy γ_{IF} using the simple formula from [25]

$$\gamma_{IF} = |\gamma_{\text{GaAs}} - \gamma_{\text{Fe}_3\text{Si}} \cdot \cos(\theta)|, \quad (3)$$

where $\gamma_{IF} \approx 100 \text{ meV } \text{\AA}^{-2}$ taking into account a contact angle $\theta \approx 33^\circ$ (figure 2), the surface energy of GaAs $\gamma_{\text{GaAs}} \approx 65 \text{ meV } \text{\AA}^{-2}$, and the surface energy of Fe_3Si $\gamma_{\text{Fe}_3\text{Si}} \approx 200 \text{ meV } \text{\AA}^{-2}$ (see above). The limited accuracy of this estimate does not allow for any conclusions about the influence of the growth rate on the interface energy.

Conclusion

Thin Fe_3Si islands and films grown on GaAs(001) exhibit long-range ordering which is depending on their growth rate. A sufficiently low enough growth rate can secure a fully ordered Fe_3Si lattice, whereas a higher growth rate leads to a nearly fully disordered film, which is however still lattice matched. The disorder occurring in the starting phase of the growth seems to be the reason for disorder observed near the $\text{Fe}_3\text{Si}/\text{GaAs}$ interface.

Acknowledgments

The authors thank V Kaganer for helpful discussion and the simulation program for the x-ray data. We also thank H Kirmse and T Heil for the help with the HAADF micrograph shown in figure 4. We are grateful C Herrmann and H-P Schönherr for their support during the growth of the samples, and D Steffen for preparation of the TEM-samples.

ORCID iDs

B Jenichen  <https://orcid.org/0000-0001-5012-1618>

Z Cheng  <https://orcid.org/0000-0002-1161-0109>

References

- [1] Volmer M and Weber A 1926 *Z. Phys. Chem.* **119** 277
- [2] Raviswaran A, Liu C-P, Kim J, Cahill D G and Gibson G 2001 *Phys. Rev. B* **63** 125314
- [3] Kaganer V M, Jenichen B, Shayduk R, Braun W and Riechert H 2009 *Phys. Rev. Lett.* **102** 016103
- [4] Placidi E, Fanfoni M, Archiprete F, Patella F, Motta N and Balzarotti A 2000 *Mater. Sci. Eng. B* **69–70** 243
- [5] Moll N, Kley A, Pehlke E and Scheffler M 1996 *Phys. Rev. B* **54** 8844
- [6] Hafner J and Spisák D 2007 *Phys. Rev. B* **75** 195411
- [7] Herfort J, Schönherr H-P and Ploog K H 2003 *Appl. Phys. Lett.* **83** 3912
- [8] Herfort J, Schoenherr H P, Friedland K J and Ploog K H 2004 *J. Vac. Sci. Technol. B* **22** 2073
- [9] Jenichen B, Kaganer V M, Herfort J, Satapathy D K, Schönherr H P, Braun W and Ploog K H 2005 *Phys. Rev. B* **72** 075329
- [10] Niculescu V, Raj K, Budnick J I, Burch T J, Hines W A and Menotti A H 1976 *Phys. Rev. B* **14** 4160
- [11] Hongzhi L, Zhiyong Z, Li M, Shifeng X, Heyan L, Jingping Q, Yangxian L and Guangheng W 2007 *J. Phys. D: Appl. Phys.* **40** 7121
- [12] Noor S, Barsukov I, Ozkan M S, Elbers L, Melnichak N, Lindner J, Farle M and Koehler U 2013 *J. Appl. Phys.* **113** 103908
- [13] Jenichen B, Kaganer V M, Braun W, Herfort J, Shayduk R and Ploog K H 2007 *Thin Solid Films* **515** 5611
- [14] Jenichen B, Kaganer V M, Braun W, Shayduk R, Tinkham B P and Herfort J 2008 *J. Mat. Sci.: Mater. Electron.* **19** 199
- [15] Ionescu A *et al* 2005 *Phys. Rev. B* **71** 094401
- [16] Herfort J, Schönherr H-P, Kawaharazuka A, Ramsteiner M and Ploog K H 2005 *J. Cryst. Growth* **278** 666
- [17] Gusenbauer C, Ashraf T, Stangl J, Hesser G, Plach T, Meingast A, Kothleitner G and Koch R 2011 *Phys. Rev. B* **83** 035319
- [18] Krumme B *et al* 2009 *Phys. Rev. B* **80** 144403
- [19] Liou S H, Malhotra S S, Shen J X, Hong M, Kwo J, Chen H S and Mannaerts J P 1993 *J. Appl. Phys.* **73** 6766
- [20] Herfort J, Schönherr H-P and Jenichen B 2008 *J. Appl. Phys.* **103** 07B506
- [21] Jenichen B, Braun W, Kaganer V M, Shtukenberg A G, Däweritz L, Schulz C G and Ploog K H 2003 *Rev. Sci. Instrum.* **74** 1267
- [22] Stadelmann P 2016 JEMS - Electron Microscopy Software Java Version, © Pierre Stadelmann 2014–2019, version 4. xx, Lausanne
- [23] Pennycook S J and Jesson D E 1990 *Phys. Rev. Lett.* **64** 938
- [24] Hashimoto M, Trampert A, Herfort J and Ploog K H 2007 *J. Vac. Sci. Technol. B* **25** 1453
- [25] de Gennes P G 1985 *Rev. Mod. Phys.* **57** 827